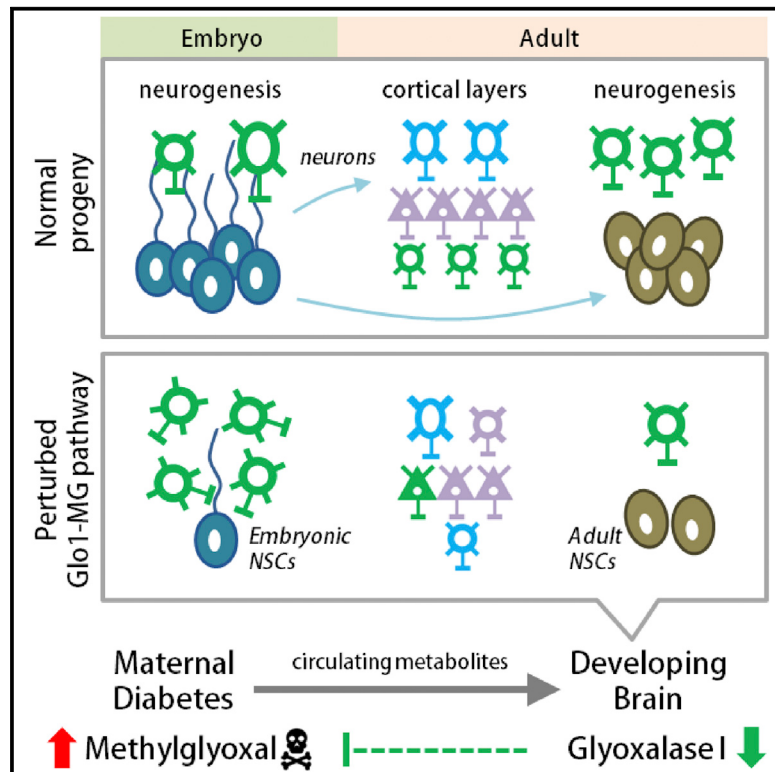


A Glo1-Methylglyoxal Pathway that Is Perturbed in Maternal Diabetes Regulates Embryonic and Adult Neural Stem Cell Pools in Murine Offspring

Graphical Abstract



Authors

Guang Yang, Gonzalo I. Cancino, Siraj K. Zahr, ..., Paul W. Frankland, David R. Kaplan, Freda D. Miller

Correspondence

dkaplan@sickkids.ca (D.R.K.), fredam@sickkids.ca (F.D.M.)

In Brief

Maternal diabetes is associated with cognitive deficits in offspring. Yang et al. show that a Glo1-methylglyoxal pathway perturbed in gestational diabetes regulates neural precursors in the developing murine cortex. Genetic or maternal environmental perturbation of this pathway in embryonic precursors also leads to long-term neuroanatomical and behavioral changes in adult offspring.

Highlights

- Glo1 regulates embryonic cortical precursor maintenance and neurogenesis
- Glo1 regulates neural precursor maintenance by metabolizing methylglyoxal
- Increased maternal methylglyoxal perturbs NPCs in embryonic and adult offspring
- Maternal diabetes similarly perturbs embryonic and adult NPCs in offspring

Accession Numbers

GSE79737



A Glo1-Methylglyoxal Pathway that Is Perturbed in Maternal Diabetes Regulates Embryonic and Adult Neural Stem Cell Pools in Murine Offspring

Guang Yang,¹ Gonzalo I. Cancino,¹ Siraj K. Zahr,^{1,5} Axel Guskjolen,^{1,2} Anastassia Voronova,¹ Denis Gallagher,¹ Paul W. Frankland,^{1,2,3,5} David R. Kaplan,^{1,4,5,*} and Freda D. Miller^{1,2,4,5,6,*}

¹Program in Neurosciences and Mental Health, Hospital for Sick Children, Toronto, ON M5G 0A4, Canada

²Department of Physiology

³Department of Psychology

⁴Department of Molecular Genetics

⁵Institute of Medical Science

University of Toronto, Toronto, ON M5G 1A8, Canada

⁶Lead Contact

*Correspondence: dkaplan@sickkids.ca (D.R.K.), fredam@sickkids.ca (F.D.M.)

<http://dx.doi.org/10.1016/j.celrep.2016.09.067>

SUMMARY

Maternal diabetes is known to adversely influence brain development in offspring. Here, we provide evidence that this involves the circulating metabolite methylglyoxal, which is increased in diabetes, and its detoxifying enzyme, glyoxalase 1 (Glo1), which when mutated is associated with neurodevelopmental disorders. Specifically, when Glo1 levels were decreased in embryonic mouse cortical neural precursor cells (NPCs), this led to premature neurogenesis and NPC depletion embryonically and long-term alterations in cortical neurons postnatally. Increased circulating maternal methylglyoxal caused similar changes in embryonic cortical precursors and neurons and long-lasting changes in cortical neurons and NPCs in adult offspring. Depletion of embryonic and adult NPCs was also observed in murine offspring exposed to a maternal diabetic environment. Thus, the Glo1-methylglyoxal pathway integrates maternal and NPC metabolism to regulate neural development, and perturbations in this pathway lead to long-lasting alterations in adult neurons and NPC pools.

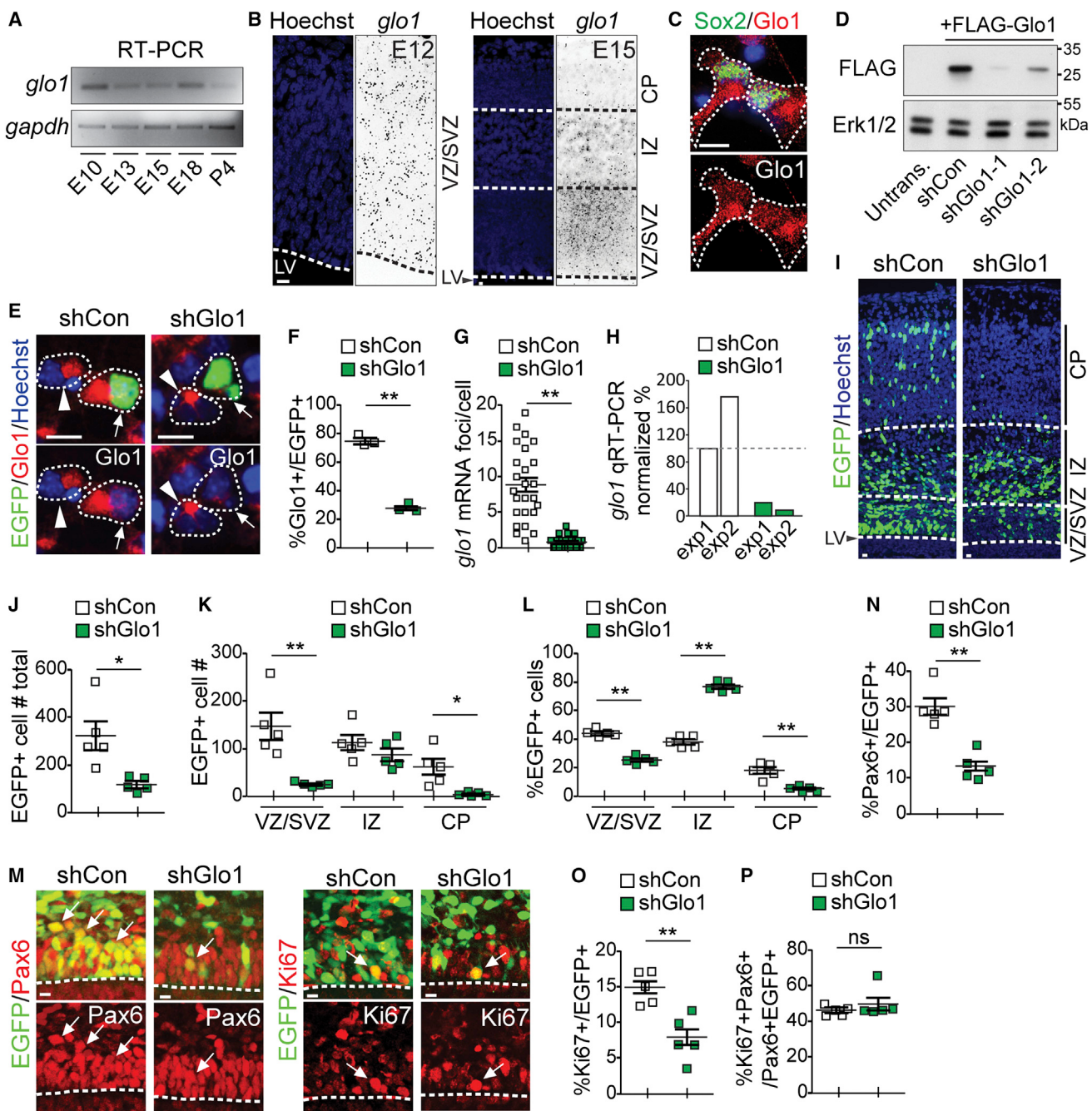
INTRODUCTION

Recent work indicates that environmental factors determine both the establishment and maintenance of adult tissue stem cell pools. As one example, adult murine neural precursor cell (NPC) numbers decrease with aging, but this decrease can be partially rescued by factors found in the circulation of young mice (Villeda et al., 2011). As a second example, transient embryonic exposure to a surge of circulating maternal interleukin 6 (IL-6) enhances self-renewal of developing forebrain NPCs

ultimately resulting in increased adult NPCs in adult offspring (Gallagher et al., 2013). Thus, systemic factors, including those in the maternal environment, play a role in determining tissue stem cell pools.

What systemic compounds regulate stem cell biology? Most studies have focused on growth factors and cytokines, but the circulation also communicates metabolic status throughout the organism, and we now know that the metabolic state regulates stem cell biology (Mihaylova et al., 2014). We therefore asked if the maternal metabolic state might regulate NPC pools, focusing on gestational diabetes, which in human offspring has been associated with neurodevelopmental disorders such as autism (Krakowiak et al., 2012; Xiang et al., 2015; Li et al., 2016). In gestational diabetes, hyperglycemia induces an overproduction of methylglyoxal, a circulating toxic intermediate metabolite that enters the fetal circulation and crosses cell membranes (Merigq et al., 2010; Rabbani and Thornalley, 2015). Intracellular methylglyoxal is metabolized by glyoxalase 1 (Glo1), the rate-limiting enzyme in the glyoxalase pathway (Rabbani and Thornalley, 2015). Intriguingly, genetic studies have identified Glo1 polymorphisms that alter enzyme activity, and these are associated with autism spectrum disorder (ASD) and schizophrenia (Junaid et al., 2004; Gabriele et al., 2014; Arai et al., 2010; Barua et al., 2011). Thus, a Glo1-methylglyoxal pathway might provide one way that normal and perturbed maternal metabolism could influence developing NPCs.

To test this idea, we studied embryonic murine cortical precursors, some of which persist to become adult forebrain NPCs (Merkle et al., 2004; Gallagher et al., 2013). We show that Glo1 is necessary to maintain the undifferentiated NPC state and that when Glo1 levels were decreased or circulating maternal methylglyoxal was increased, this caused premature neurogenesis and depletion of embryonic NPCs. Moreover, embryonic exposure to increased maternal methylglyoxal caused long-lasting decreases in adult NPC numbers and neurogenesis, cortical neuron perturbations, and aberrant behaviors. Finally, we show that similar perturbations in embryonic and adult NPCs occur

**Figure 1. Gloc1 Is Essential for Maintaining Cortical Radial Precursors**(A) RT-PCR for *glo1* mRNA in cortices from E10 to P4. *gapdh* mRNA served as an internal control.(B) Single-molecule FISH for *glo1* mRNA (shown as black on white) in coronal sections of E12 (left) and E15 (right) cortex. LV, lateral ventricle.

(C) E12/E13 cortical precursors cultured 3 days and immunostained for Glo1 (red) and Sox2 (green). Hatched lines are cell boundaries.

(D) Western blots of HEK293 cells cotransfected with plasmids encoding FLAG-tagged mouse Glo1, with or without one of two Glo1 shRNAs (shGlo1-1 and shGlo1-2) or a control shRNA (shCon), probed with anti-FLAG and reprobed with anti-Erk1/2. Untransfected (Untrans.) cells served as a control. Molecular weight markers are indicated to the right.

(E and F) Cultured E12/E13 precursors were cotransfected with EGFP and control shRNA (Con) or Glo1 shRNA-1 (shGlo1) and immunostained for Glo1 (red) and EGFP (green) after 2 days (E), and the relative proportion of EGFP-positive cells expressing detectable Glo1 was determined (F). Arrows and arrowheads denote EGFP-positive and negative cells, respectively. Each scatterplot point represents the mean signal in an individual experiment. ***p* < 0.01.(G and H) E13/E14 cortices were coelectroporated with nuclear EGFP and control (Con) or Glo1-1 (shGlo1) shRNAs. In (G), sections were immunostained for EGFP and analyzed by FISH for *glo1* mRNA 3 days later (see Figure S1A) and the number of *glo1* mRNA foci per individual EGFP-positive cell determined.

(legend continued on next page)

in a gestational diabetes model. Thus, the maternal metabolic state regulates NPC development via the Glo1-methylglyoxal pathway, suggesting that Glo1 polymorphisms and/or gestational diabetes might predispose humans to cognitive dysfunction by perturbing this pathway in developing NPCs.

RESULTS

Glo1 Is Essential for Maintaining NPCs in the Developing Cortex

We first analyzed Glo1 expression in the embryonic murine cortex. RT-PCR showed that *glo1* mRNA was expressed from embryonic day 10 (E10), when the cortex largely consists of proliferating precursors, until postnatal day 4 (P4) (Figure 1A). Single-molecule fluorescent *in situ* hybridization (FISH) (Figure 1B) showed that at E12, *glo1* mRNA was expressed throughout the cortex, while at E15, it was enriched in the ventricular and subventricular precursor zones (VZ/SVZ), with lower levels in the intermediate zone (IZ) and the cortical plate (CP), regions containing newborn neurons. Immunostaining of cultured E12.5 cortical precursors also revealed detectable Glo1 in Sox2-positive cells (Figure 1C).

To ask about Glo1 function in cortical precursors, we utilized a Glo1 small hairpin RNA (shRNA) (shGlo1-1) that decreased FLAG-tagged murine Glo1 when cotransfected into HEK293 cells (Figure 1D). Three approaches showed that this shRNA was efficacious in cortical precursors. First, immunostaining of cultured precursors cotransfected with an EGFP plasmid and control or Glo1 shRNAs showed that Glo1 knockdown markedly reduced the proportion of transfected cells expressing detectable Glo1 (Figures 1E and 1F). Second, we used *in utero* electroporation at E13/E14 to transfect cortical radial precursors that line the lateral ventricles with cytoplasmic EGFP and control or Glo1 shRNAs. Immunostaining for EGFP combined with FISH for *glo1* mRNA showed that Glo1 knockdown significantly decreased *glo1* mRNA foci per EGFP-positive cell (Figure 1G; Figure S1A). Third, we used fluorescence-activated cell sorting (FACS) and qRT-PCR to show that *glo1* mRNA was decreased in E15/E16 cortical cells that were electroporated with EGFP and Glo1 shRNA at E13/E14 (Figure 1H).

We then used this shRNA to ask if Glo1 knockdown altered cortical development. E13/E14 cortices were electroporated with nuclear EGFP and control or Glo1 shRNAs and immunostained 3 days later for EGFP and cell-type-specific markers (Figure 1I; Figures S1B and S1C). This analysis showed that there was a decreased total number of EGFP-positive cells following Glo1 knockdown (Figures 1I and 1J) and that their distribution was altered, with significant decreases in the total numbers of EGFP-positive cells in the VZ/SVZ and CP, when expressed

either as total cells or as a proportion of the total number of EGFP-positive cells (Figures 1I, 1K, and 1L). There were also fewer EGFP-positive cells expressing the radial precursor marker Pax6 or the proliferation marker Ki67 (Figures 1M–1O), although the proliferation index (the proportion of Pax6-positive cells that also expressed Ki67) was unaltered (Figure 1P). Immunostaining for the apoptosis marker cleaved caspase-3 showed that these changes were not due to enhanced cell death (Figure S1D).

One explanation for the observed depletion of radial precursors was that Glo1 knockdown caused premature differentiation of precursors into neurons. We tested this idea, immunostaining similar electroporated sections for Tbr2, a marker for neurogenic intermediate progenitors, for the neuronal marker β III-tubulin, or for Satb2, a transcription factor expressed in almost all neurons born over the time frame of our electroporations (Tsui et al., 2013) (Figure 2A; Figure S2A). Glo1 knockdown significantly increased both intermediate progenitors (Figure 2B) and newborn neurons (Figure 2C). Intriguingly, almost all EGFP-positive, Satb2-positive neurons were aberrantly located in the IZ (Figure 2D), explaining the decrease in EGFP-positive cells in the CP (Figures 1I, 1K, and 1L). Thus, Glo1 knockdown caused premature neurogenesis, and these new neurons were mislocalized.

Glo1 Is Sufficient to Promote Radial Precursor Maintenance

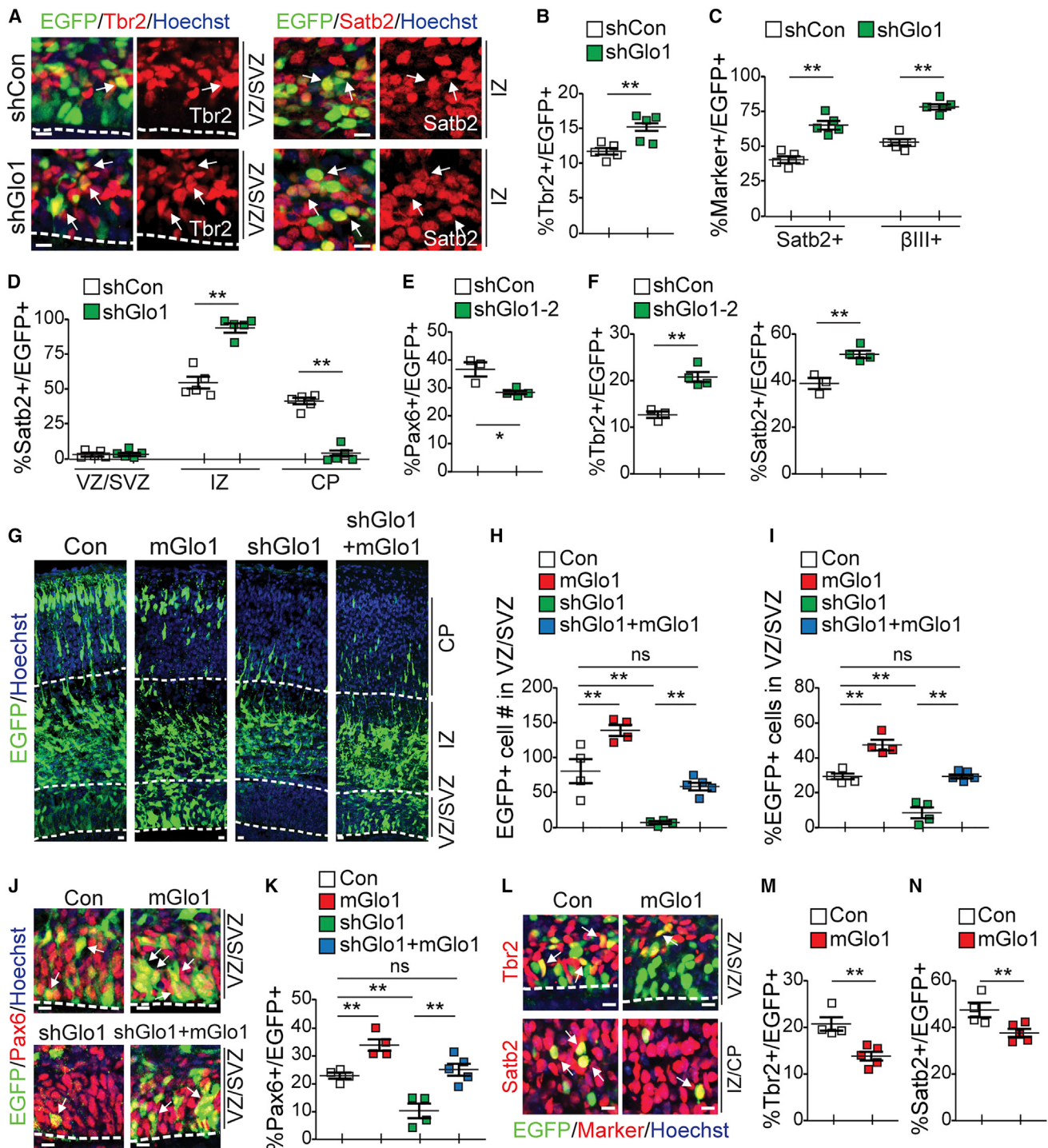
To ensure the specificity of the knockdown phenotypes, we performed two sets of experiments. First, we electroporated E13/E14 cortices with a second Glo1 shRNA (shGlo1-2 in Figure 1D). Analysis 3 days later showed that shGlo1-2 depleted EGFP-positive, Pax6-positive radial precursors and increased Tbr2-positive intermediate progenitors and Satb2-positive neurons (Figures 2E and 2F). Second, we performed rescue experiments, electroporating E13/E14 cortices with Glo1 shRNA with or without an expression vector for Glo1 engineered so that it was resistant to the shRNA (Figure S2B). For comparison, we electroporated the Glo1 expression vector alone. Analysis 3 days later showed that ectopic Glo1 expression rescued the decrease in *glo1* mRNA caused by the Glo1 shRNA (Figure S2C). It also rescued the Glo1 shRNA-mediated decrease in EGFP-positive cells in the VZ/SVZ (Figures 2G–2I) and the depletion of EGFP-positive, Pax6-positive radial precursor cells (Figures 2J and 2K).

These experiments validated the specificity of the Glo1 knockdowns. However, they also showed that Glo1 overexpression alone increased EGFP-positive cells in the VZ/SVZ and EGFP-positive, Pax6-positive radial precursors (Figures 2G–2K). We therefore asked if increased Glo1 levels also affected neurogenesis. Immunostaining 3 days following electroporation with a

** $p < 0.01$; n = 25 EGFP-positive cells each. In (H), EGFP-positive cells were isolated by FACS 2 days post-electroporation and analyzed by qPCR for *glo1* mRNA, with values normalized to *gapdh* mRNA. The graph shows two experiments (exp1 and exp2), each involving five or six embryos per group.

(I–P) E13/E14 cortices were coelectroporated as in (G) and (H) and coronal cortical sections analyzed 3 days later. (I) Representative EGFP-immunostained sections. (J–L) Scatterplots showing (J) the number of EGFP-positive cells in a column spanning the cortex or (K) the number or (L) proportion of EGFP-positive cells in the different cortical regions (see Figures S1B and S1C). * $p < 0.05$, ** $p < 0.01$, n = 5 embryos each. (M) The VZ/SVZ immunostained for EGFP (green) and Pax6 (red, left) or Ki67 (red, right). Arrows denote double-labeled cells. (N–P) Quantification of sections as in (M) for EGFP-positive cells expressing Pax6 (N) or Ki67 (O) and for the ratio of EGFP-positive, Pax6-positive cells also positive for Ki67 (P). ** $p < 0.01$, ns = p > 0.05; n = 5 embryos each. For (J)–(L) and (N)–(P), each scatterplot point represents mean cell numbers from three sections of an individual embryo.

Sections in (B), (C), (E), and (I) were counterstained with Hoechst 33258 (blue). Scale bars, 10 μ m. Error bars denote SEM. See also Figure S1.

**Figure 2. Glo1 Promotes Maintenance of Radial Precursors**

(A–F) E13/E14 cortices were analyzed 3 days following electroporation with nuclear EGFP and control shRNA (Con), Glo1-1 shRNA (shGlo1) (A–D), or Glo1-2 shRNA (shGlo1-2) (E and F). (A) The VZ/SVZ (left) and IZ (right) immunostained for EGFP (green) and Tbr2 (red, left) or Satb2 (red, right). Ventricles are outlined, and arrows denote double-labeled cells. (B–F) Quantification of images as in (A) for EGFP-positive cells expressing cell-type-specific markers (B, C, E, and F) or for the distribution of EGFP-positive, Satb2-positive cells (D). * $p < 0.05$; ** $p < 0.01$; n = 3–5 embryos.

(G–K) E13/E14 cortices were analyzed 3 days following electroporation with cytoplasmic EGFP and control (Con) or Glo1-1 (shGlo1) shRNA plus or minus shRNA-resistant murine Glo1 (mGlo1). (G–I) Sections were immunostained for EGFP (green, G), and the total number (H) or relative proportion (I) of EGFP-positive VZ/SVZ cells was determined. ** $p < 0.01$, ns = p > 0.05. n = 4–5 embryos. (J and K) The VZ/SVZ was immunostained for EGFP (green, J) and Pax6 (red, J), and the

(legend continued on next page)

murine Glo1 expression plasmid and EGFP showed that Tbr2-positive intermediate progenitors and Satb2-positive newborn neurons were both decreased by Glo1 overexpression (Figures 2L–2N). Thus, Glo1 overexpression decreases neurogenesis and enhances radial precursor maintenance.

Decreased Glo1 in Cortical Precursors Causes Postnatal Perturbations in Cortical Neurons

To ask if these embryonic perturbations had long-term consequences, we electroporated cortices at E13/14 and analyzed them at P3/P4 (Figure S3A). Immunostaining for EGFP revealed that Glo1 knockdown caused mislocalization of postnatal EGFP-positive cells (Figures 3A and 3B). In controls, most EGFP-positive cells were in layers II–IV, while with Glo1 knockdown, most were located in layers V/VI (Figures 3A and 3B). Immunostaining for the neuronal marker NeuN (Figure S3B) showed that almost all of these EGFP-positive cells were neurons (control, 88.9% \pm 0.4%; shGlo1, 88.5% \pm 1.8%).

We characterized the phenotype of these mislocalized neurons by immunostaining for Cux1 and Ctip2, which mark neurons in layers II–IV and layer V, respectively (Figures 3A–3D). In controls, almost 90% of EGFP-positive cells were Satb2 positive, and only ~2% were Ctip2 positive. Glo1 knockdown caused a modest but significant decrease in Satb2-positive neurons and a coincident increase in Ctip2-positive neurons. However, while the Ctip2-positive cells were appropriately located in layer V, following Glo1 knockdown, the majority of the EGFP-positive, Satb2-positive cells were aberrantly located in layers V/VI rather than in layers II–IV (Figures 3C and 3E). Thus, embryonic Glo1 knockdown altered the location and, to some extent, phenotype of postnatal cortical neurons.

Increased Circulating Maternal Methylglyoxal Dere-regulates Embryonic Neural Precursors

Glo1 is the rate-limiting enzyme responsible for detoxifying methylglyoxal (Figure 3F). Since in gestational diabetes methylglyoxal is increased in both the maternal and fetal circulations (Ankrah and Appiah-Opong, 1999; Mericq et al., 2010), we asked whether circulating maternal methylglyoxal might deregulate embryonic NPCs. We injected pregnant mothers intraperitoneally twice daily with methylglyoxal commencing at gestational day 12 (G12)/G13 and injected them once with bromodeoxyuridine (BrdU) at G13/G14 to label proliferating NPCs. These injections had no effect on maternal weight (Figure S3C). Analysis of cortices from their E16/E17 embryonic progeny (Figures 3G–3J) demonstrated that increased maternal methylglyoxal decreased the proportion of BrdU-positive cells in the VZ/SVZ as well as BrdU-positive, Pax6-positive radial precursors.

Two lines of evidence indicated that this precursor depletion was due to an increase in methylglyoxal in cortical precursors.

First, we electroporated E13/E14 cortices with nuclear EGFP while at the same time injecting methylglyoxal into the lateral ventricles to increase its concentration locally. Analysis 2 days later (Figures 3K–3O) showed that local methylglyoxal significantly decreased EGFP-positive cells in the VZ/SVZ and EGFP-positive, Pax6-positive radial precursors while coincidentally increasing EGFP-positive, Satb2-positive neurons (Figures 3K–3O). Second, we asked if increasing Glo1 levels (and thus methylglyoxal clearance) in radial precursors would rescue the effects of increased maternal methylglyoxal. We electroporated E13/E14 cortices with cytoplasmic EGFP and either a control or mouse Glo1 expression plasmid, injected mothers daily with methylglyoxal commencing 1 day later, and analyzed cortices at E17/E18 (Figures 4A–4D; Figure S4A). Consistent with the BrdU studies (Figure 3G–3J), increased maternal methylglyoxal decreased EGFP-positive VZ/SVZ cells and EGFP-positive, Pax6-positive radial precursors and increased EGFP-positive, Satb2-positive neurons. All of these phenotypes were rescued by coincident electroporation of the Glo1 expression plasmid (Figures 4A–4D), providing evidence that they were due to increased intracellular methylglyoxal.

The Glo1-Methylglyoxal Pathway Regulates Apical Localization of Radial Precursors

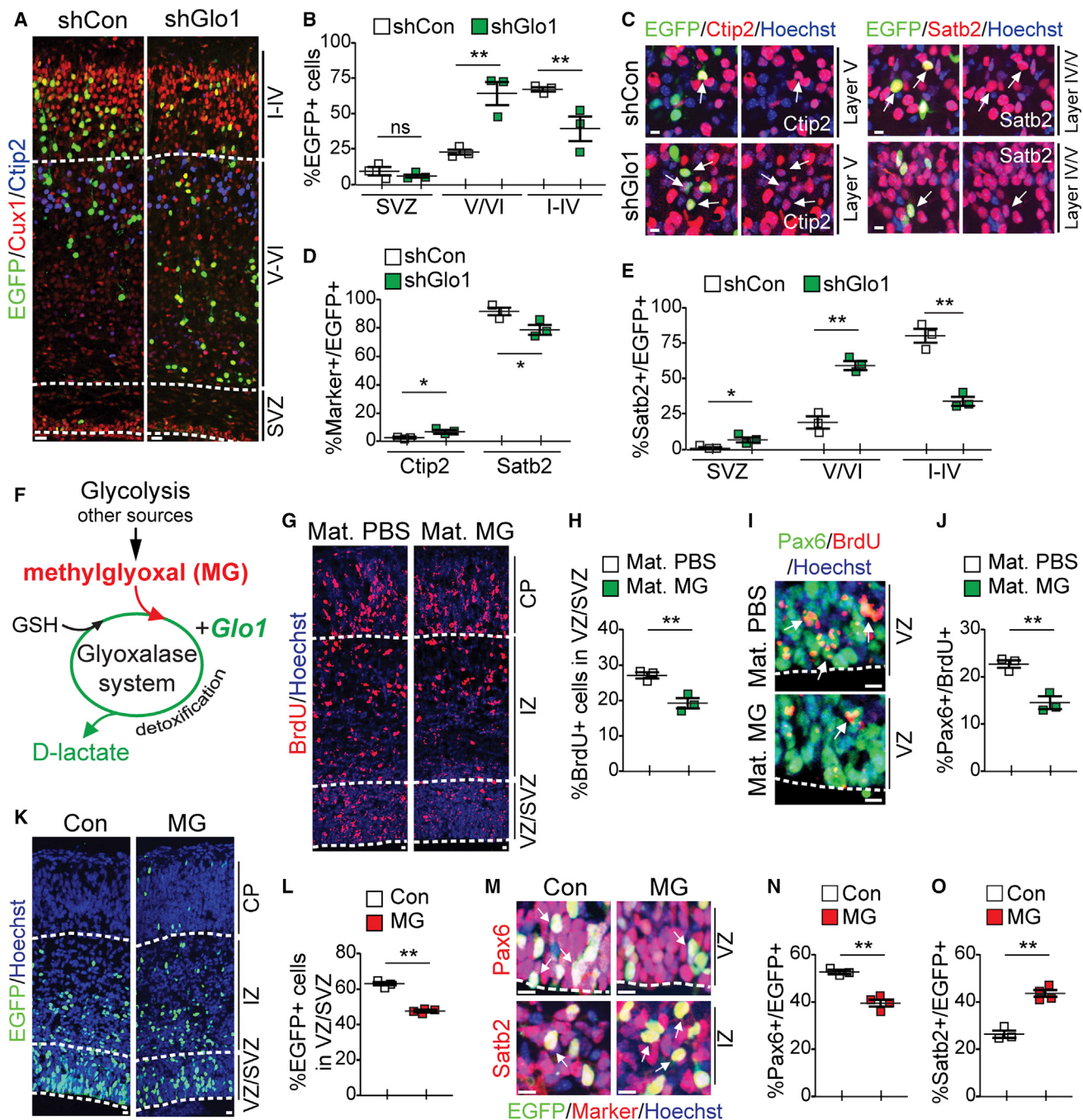
We next asked how the Glo1-methylglyoxal pathway might regulate neurogenesis by examining radial precursors in more detail 3 days following electroporation with EGFP and control or Glo1 shRNAs. In controls, almost all EGFP-positive, Pax6-positive, or Ki67-positive cells were located in the VZ, but following Glo1 knockdown, almost half of the Pax6-positive cells were outside of the VZ, and many of these were Ki67 positive (Figures 4E and 4F). Immunostaining for the mitotic marker phospho-histone H3 (pH3) also demonstrated mislocalization of dividing precursors. Specifically, analysis 2 days post-electroporation showed that in controls, almost all EGFP-positive, pH3-positive cells were at the apical ventricular surface, but following Glo1 knockdown, ~60% were aberrantly located outside of the apical VZ (Figure 4G).

To ask if this basal mislocalization was due to detachment from the apical ventricular surface, we analyzed precursor morphology 2 days post-electroporation with membrane-targeted EGFP. In controls, almost 70% of transfected Pax6-positive cells had EGFP-positive endfeet integrated into the apical ventricular surface. However, following Glo1 knockdown, this was reduced to 40%, with many Pax6-positive, EGFP-positive cells delaminated from the apical surface (Figures 4H and 4I). Immunostaining for two proteins associated with apical endfeet, atypical PKC (aPKC) and Par3, confirmed this detachment (Figure 4J). These delaminated cells were precursors, since they expressed Pax6 and nestin, but not β III-tubulin (Figure S4B).

proportion of EGFP-positive cells expressing Pax6 was determined (K). Ventricles are outlined, and arrows denote double-labeled cells. ** $p < 0.01$, ns = $p > 0.05$; n = 4–5 embryos.

(L–N) E13/E14 cortices were electroporated with nuclear EGFP and murine Glo1 (mGlo1) and immunostained for EGFP (green) and Tbr2 (red, top L) or Satb2 (red, bottom L) 3 days later, and the proportion of EGFP-positive cells expressing Tbr2 (M) or Satb2 (N) was determined. Top and bottom panels in (L) show the VZ/SVZ and iZ/CP, respectively, and arrows denote double-labeled cells. ** $p < 0.01$; n = 4–5 embryos. In scatterplots, single points represent the mean cell numbers from three sections of an individual embryo.

Sections in (A), (G), (J), and (L) were counterstained with Hoechst 33258 (blue). Scale bars, 10 μ m. Error bars denote SEM. See also Figure S2.

**Figure 3. Effects of *Glo1* Knockdown and Circulating Maternal Methylglyoxal on the Postnatal and Embryonic Cortex**

(A–E) E13/E14 cortices were electroporated with nuclear EGFP and control (Con) or *Glo1*-1 (sh*Glo1*) shRNAs and analyzed at P4. (A and B) Sections immunostained for EGFP (green, A), Cux1 (red, A), and Ctip2 (blue, A) were analyzed for the distribution of EGFP-positive cells in the different cortical layers (B). **p < 0.01, ns = p > 0.05; n = 3 animals each. (C–E) Sections immunostained for EGFP (green, C) and Ctip2 (red, left) or Satb2 (red, right) were analyzed for the proportions of EGFP-positive cells expressing the markers (D) or for EGFP-positive, Satb2-positive cells in the different cortical layers (E). *p < 0.05, **p < 0.01; n = 3 animals each.

(F) Schematic of the *Glo1*-methylglyoxal pathway. Methylglyoxal accumulates inside cells from extracellular sources and as a by-product of glycolysis. *Glo1* and *Glo2* detoxify methylglyoxal to D-lactate, with glutathione (GSH) as a cofactor.

(G–J) G13/G14 mothers were injected with methylglyoxal (Mat. MG) or PBS (Mat. PBS) and BrdU, and 3 days later, embryonic cortices were immunostained for BrdU (red, G and I) and Pax6 (green, I) and analyzed for the percentage of BrdU-positive cells in the VZ/SVZ (H) or expressing Pax6 (J). **p < 0.01; n = 3 embryos each.

(legend continued on next page)

We next asked whether a similar mislocalization of radial precursors might occur in response to maternal methylglyoxal. We administered methylglyoxal or vehicle to pregnant mice commencing at G12/G13, injected them with BrdU at G14/G15, and analyzed embryos 30 min later. In controls, almost all BrdU-positive cells were Pax6-positive radial precursors, and only 8% were Tbr2-positive intermediate progenitors (Figures 4K and 4L). Maternal methylglyoxal modestly decreased BrdU-positive radial precursors with a coincident increase in intermediate progenitors (Figures 4K and 4L). However, maternal methylglyoxal also caused a 2- to 3-fold increase in BrdU-positive cells located outside of the VZ, most of which were Pax6-positive radial precursors (Figures 4M–4O). Since increased neurogenesis also occurs following experimentally induced apical detachment (Das and Storey, 2014), then the apical detachment observed here likely explains the premature neurogenesis caused by perturbing the Glio1-methylglyoxal pathway.

Increased Maternal Methylglyoxal Has Long-Term Effects on Adult NPCs and Neurogenesis

We next asked whether embryonic exposure to maternal methylglyoxal had long-term neural consequences, initially focusing on forebrain subventricular zone (SVZ) NPCs, since some embryonic cortical precursors persist to partially populate this niche (Merle et al., 2004; Gallagher et al., 2013). Specifically, pregnant mice were injected with methylglyoxal from G12/G13 to delivery, and their 2-month-old adult offspring were injected with BrdU. Analysis 1 day later showed that maternal methylglyoxal decreased the total number of BrdU-positive adult SVZ cells and the proportion of Sox2-positive NPCs that were BrdU positive (Figures 5A–5C). Adult-born BrdU-positive, NeuN-positive neurons from the SVZ were also decreased, as shown by analysis of the olfactory bulbs of 2-month-old offspring injected with BrdU 1 month previously (Figures 5D and 5E).

We characterized these deficits further by culturing SVZ NPC neurospheres from adult mice that were or were not exposed to maternal methylglyoxal as embryos. Quantification showed that fewer primary neurospheres were generated from the SVZ of methylglyoxal-exposed mice and that, when passaged, these neurosphere cells generated fewer secondary neurospheres (Figure 5F). Differentiation of the primary neurospheres (Figure S5) showed that similar numbers of neurons and glial cells were generated from both groups: ~20% were β III-tubulin-positive neurons (PBS offspring, $21.9\% \pm 2.6\%$; methylglyoxal (MG) offspring, $19.0\% \pm 7.9\%$; $p = 0.74$, $n = 3$), <2.5% were myelin basic protein (MBP)-positive oligodendrocytes, and the remainder were GFAP-positive astrocytes. Finally, we analyzed RNA from three independent biological replicates of each group of primary neurospheres on Affymetrix GeneChip Mouse Gene 2.0 ST arrays. Spearman rank correlation of the ranked microarray expression data using all probe sets demonstrated that the different biological replicates for each group clustered together

and that the two populations were highly similar (Figure 5G). Differential gene expression using Partek Genomics Suite software confirmed this similarity, showing that only 183 annotated genes were differentially expressed ($p < 0.05$) (Table S1), with mean changes of only ± 1.3 -fold (Figure 5H), suggesting that exposure to increased maternal methylglyoxal during embryogenesis did not qualitatively affect adult NPCs.

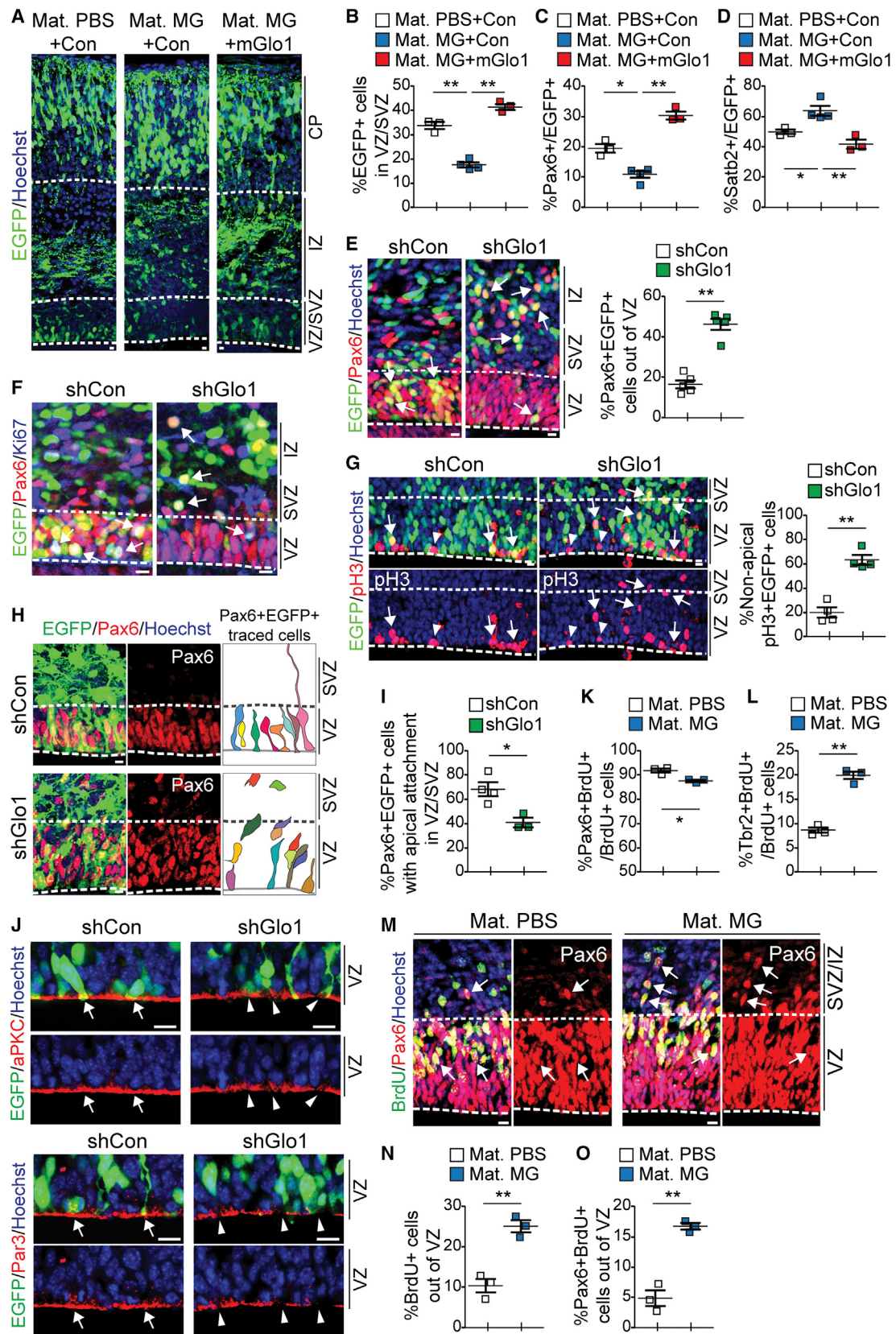
These data demonstrate that embryonic exposure to maternal methylglyoxal caused a long-term decrease in SVZ NPCs. We asked if this was reflective of a general decrease in adult NPCs by analyzing the subgranular zone (SGZ) of the hippocampal dentate gyrus 1 day following BrdU injection into adult offspring. This analysis showed that maternal methylglyoxal caused a decrease in Sox2-positive NPCs, BrdU-positive cells, and double-labeled BrdU-positive, Sox2-positive proliferating NPCs in the SGZ (Figures 5I–5L). Adult neurogenesis was also decreased, as indicated by quantifying SGZ cells expressing the newborn neuron marker doublecortin (DCX) (Figure 5M). We confirmed this decrease in adult-born neurons by quantifying BrdU-positive, NeuN-positive dentate gyrus neurons in 2-month-old offspring injected with BrdU 1 month previously (Figure 5N).

Maternal Methylglyoxal Has Long-Term Effects on the Adult Mouse Cortex and Adult Behavior

We next asked whether maternal methylglyoxal had long-term consequences for the adult cortex. To do so, we injected pregnant mice with methylglyoxal from G12/G13 until delivery, injected them with BrdU on G13/G14, and then analyzed their adult offspring, which displayed normal weight gain over the postnatal period (Figure S3D). Immunostaining of the adult cortex for BrdU (Figures 6A and 6B; Figures S6A and S6B), showed that total cortical thickness was unaffected by maternal methylglyoxal (Figure 6C). However, the total number of BrdU-labeled cells was decreased, as determined by counting labeled cells in equivalently sized columns spanning the cortical layers (Figure 6D). The distribution of these BrdU-positive cells was also different, with fewer in layers V/VI and the bottom half of layer II–IV (Figure 6E).

We characterized the phenotype of these BrdU-positive cells by immunostaining for Satb2 and/or Cux1, which are expressed in neurons of cortical layers II–IV that are born around the time we injected BrdU (Figures 6A and 6B; Figures S6A and S6B). In both controls and maternal methylglyoxal offspring, ~80%–90% of BrdU-positive cells were Satb2-positive neurons (compare Figures 6D and 6F). Approximately half of these BrdU-positive, Satb2-positive neurons coexpressed Cux1 ($59.7\% \pm 4.2\%$ versus $55.3\% \pm 5.7\%$, controls versus maternal methylglyoxal). However, there were only approximately half as many BrdU-positive, Satb2-positive neurons in mice exposed to maternal methylglyoxal (Figure 6F). Moreover, even the total numbers of Satb2-positive and Cux1-positive neurons were decreased (Figure 6G).

(K–O) E13/E14 cortices were electroporated with EGFP and coincidentally injected with 50 μ M methylglyoxal (MG) or PBS (Con), immunostained 2 days later for EGFP (green, K and M) and Satb2 or Pax6 (both red, M), and analyzed for the proportion of EGFP-positive cells in the VZ/SVZ (L) or expressing Pax6 (N) or Satb2 (O). ** $p < 0.01$; $n = 3$ –4 embryos. In scatterplots, single points represent the mean cell numbers from three sections of an individual embryo. Sections in (C), (G), (I), (K), and (M) were counterstained with Hoechst 33258 (blue), and arrows show double-labeled cells. Scale bars represent 50 μ m (A) or 10 μ m (C, G, I, K, and M). Error bars denote SEM. See also Figure S3.



(legend on next page)

These data indicate that there was a depletion of upper layer neurons and, consistent with this, the width of layers II–IV (defined by Cux1 immunostaining as in Figure 6B) was significantly decreased (Figure 6H). These neuronal deficits could be readily explained by maternal methylglyoxal-induced depletion of embryonic radial precursors.

We also asked if maternal methylglyoxal exposure had long-term behavioral consequences, using two assays thought to reflect neurodevelopmental perturbations. The first was a three-chamber social preference test (Crawley, 2007) where one side chamber contained an inanimate object and the other an unfamiliar mouse (stranger 1). Control and maternal methylglyoxal mice both spent more time sniffing the unfamiliar mouse (Figure 6I). However, when the inanimate object was replaced with a second unfamiliar mouse (stranger 2), control mice spent more time sniffing the new stranger 2 mouse, but maternal methylglyoxal mice showed no preference (Figure 6J). This was not due to differences in general activity, since in open field assays, both groups traveled similar distances and explored the arena equivalently (Figure 6K; Figure S6C). The second test was a marble-burying assay (Deacon, 2006) that assesses stereotypic/repetitive behaviors thought to be associated with neurodevelopmental disorders. Adult mice exposed to maternal methylglyoxal buried significantly more marbles at both 20 and 30 min in this assay (Figure 6L).

Embryonic and Adult NPCs Are Perturbed in Offspring of Mice with Gestational Diabetes

We next tested the idea that gestational diabetes, which aberrantly increases circulating maternal methylglyoxal levels, might also perturb NPCs, taking advantage of heterozygous leptin receptor mutant mice (*Lepr*^{db/+}) that, when pregnant, become glucose intolerant and display high fasting glucose levels (Yamashita et al., 2001). We crossed *Lepr*^{db/+} or wild-type females with wild-type males and injected the pregnant mice with BrdU on G13/G14. Analysis 3 days later showed that BrdU-positive, Pax6-positive radial precursors were decreased and BrdU-positive, Tbr2-positive intermediate progenitors were increased in wild-type offspring of *Lepr*^{db/+} mothers (Figures 7A–7E). Furthermore, even the total numbers of Pax6-positive and Tbr2-positive cells were decreased and increased, respectively (Figures 7F and 7G). Thus, maternal diabetes depletes embryonic radial precursors and enhances neurogenesis.

We also asked if gestational diabetes altered adult NPCs by injecting 2-month-old wild-type offspring of *Lepr*^{db/+} or wild-type mothers with BrdU. Analysis of the SVZ 1 day later showed that BrdU-positive cells were reduced in offspring of *Lepr*^{db/+} mothers, as was the proportion of Sox2-positive NPCs that were BrdU positive (Figures 7H and 7I; Figures S7A and S7B). Moreover, in the SGZ of wild-type offspring of *Lepr*^{db/+} mothers, the amount of BrdU-positive and Sox2-positive NPCs was reduced, as was the number of double-labeled NPCs (Figures 7J–7M; Figure S7C). The number of DCX-positive newborn neurons was also decreased (Figures 7N and 7O). Thus, embryonic exposure to a maternal diabetes environment caused long-term alterations in both embryonic and adult NPCs.

DISCUSSION

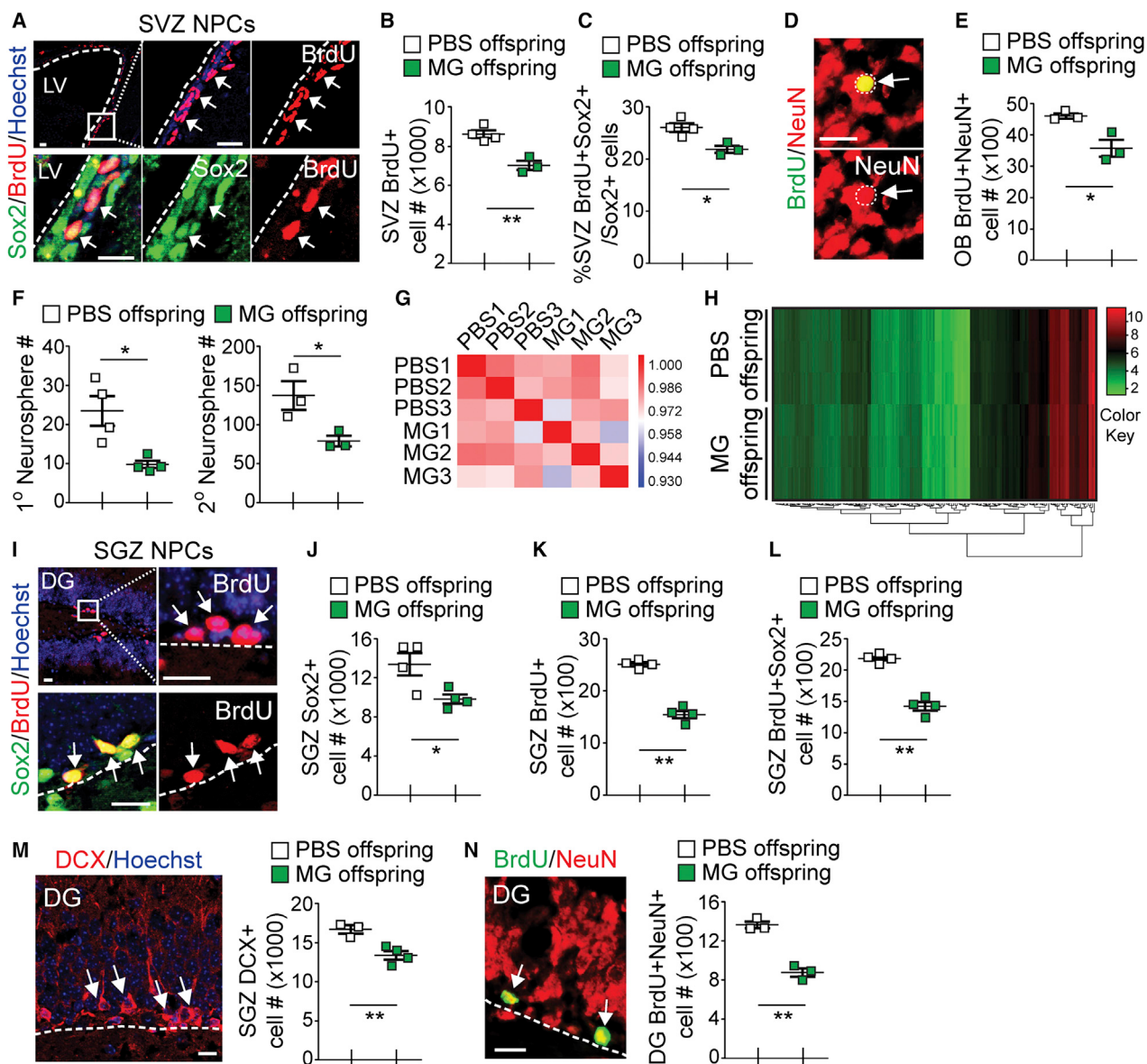
The adverse maternal environment that occurs during gestational diabetes and other metabolic disorders has a substantial impact on fetal brain development (Krakowiak et al., 2012; Xiang et al., 2015; Li et al., 2016), but the underlying mechanisms are poorly defined. Results presented here define the Glo1-methylglyoxal pathway as one way that both normal and perturbed maternal metabolic states can regulate NPCs and neurogenesis throughout life (Figure 7P). In this regard, methylglyoxal is well characterized as a circulating metabolite that contributes to diabetic complications (Sousa Silva et al., 2013). In diabetes and metabolic disorders, increased systemic methylglyoxal is thought to enter cells and overwhelm the intracellular detoxifying capacity of Glo1 and thereby cause cellular dysfunction and tissue damage. Our data are consistent with this idea, since Glo1 overexpression in embryonic radial precursors rescued the effects of increased circulating maternal methylglyoxal that is known to cross the placental barrier and rapidly enter cells. We therefore suggest that the Glo1-methylglyoxal pathway integrates maternal and embryonic NPC metabolic states and that when this goes awry, either maternally or from Glo1 mutation, it causes increased intracellular methylglyoxal, aberrant NPC development, and long-term neuroanatomical and functional alterations. In this regard, neurodevelopmental disorders are thought to result from the interplay between the environment and genetic vulnerability, and our data define the Glo1-methylglyoxal pathway as one substrate for this interaction.

Figure 4. Excessive Methylglyoxal Causes Radial Precursors to Delaminate from the Apical VZ

(A–D) E13/E14 embryos were electroporated with cytoplasmic EGFP and murine Glo1 (mGlo1) or control (Con) plasmids. 1 day later, mothers were injected with methylglyoxal (Mat. MG) or PBS (Mat. PBS) for 3 days, and cortices were immunostained for EGFP (green, A) and Pax6 or Satb2 and analyzed for the proportion of EGFP-positive cells in the VZ/SVZ (B) or analyzed for the proportion that were also positive for Pax6 (C) or Satb2 (D). *p < 0.05, **p < 0.01; n = 3–4 embryos. (E–J) E13/E14 cortices were coelectroporated with nuclear EGFP (E–G) or membrane-targeted EGFP (H–J) and analyzed 2 (G–J) or 3 (E and F) days later. (E–G) Sections were immunostained for EGFP (green, E–G) and Pax6 (red, E and F), Ki67 (blue, F), or pH3 (red, G) and analyzed for the proportion of Pax6-positive, EGFP-positive cells outside of the VZ (E) or pH3-positive, EGFP-positive cells that were not apically localized (G). **p < 0.01; n = 4–5 embryos. (H–J) Sections were immunostained for EGFP (green, H and J) and Pax6 (red, H), aPKC (red, top J), or Par3 (red, bottom J) and analyzed for the proportion of Pax6-positive, EGFP-positive cells in the VZ/SVZ that had apical attachments (I). In (H), double-positive cells were traced (shown at right), and in (J), arrows and arrowheads denote intact and disrupted apical surfaces, respectively. *p < 0.05; n = 3–4 embryos.

(K–O) Embryonic cortices of mothers injected with methylglyoxal (Mat. MG) or PBS (Mat. PBS) commencing at G12/G13, with BrdU at G14/G15, immunostained for BrdU (green, M) and Pax6 (red, M) or Tbr2 0.5 hr later, and analyzed for the proportions of BrdU-positive cells expressing Pax6 (K) or Tbr2 (L) or located outside of the VZ (N) or for Pax6-positive, BrdU-positive cells located outside of the VZ (O). *p < 0.05, **p < 0.01; n = 3 embryos each. In scatterplots, single points represent the mean cell numbers from three sections of an individual embryo.

Sections in (A), (E), (G), (H), (J), and (M) were counterstained with Hoechst 33258 (blue), and arrows show double-labeled or triple-labeled (F) cells. Scale bars, 10 µm. Error bars denote SEM. See also Figure S4.

**Figure 5. Exposure to Increased Maternal Methylglyoxal Reduces Adult NPCs and Neurogenesis in Offspring**

Pregnant mice were injected with methylglyoxal (MG) or PBS from G12/G13 until delivery, and 2-month-old offspring were analyzed.

(A–C) SVZ sections from offspring injected with BrdU 1 day earlier immunostained for BrdU (red, A) and Sox2 (green, A) and analyzed for the total number of BrdU-positive SVZ cells (B) or the proportion of Sox2-positive cells also positive for BrdU (C). (A) A control brain is shown, and the boxed area is shown at higher magnification. LV, lateral ventricle. * $p < 0.05$, ** $p < 0.01$; n = 3–4 animals.

(D and E) Olfactory bulb sections from offspring injected with BrdU 1 month earlier were immunostained for BrdU (green, D) and NeuN (red, D) and the total number of BrdU-positive, NeuN-positive cells quantified (E). (D) A control brain is shown. * $p < 0.05$; n = 3 animals each.

(F) Quantification of neurospheres generated from SVZ cells cultured at one cell per microliter for 7 days later (left) and then passaged at one cell per microliter and counted for a further 7 days to generate secondary spheres (right). * $p < 0.05$; n = 3–4 animals.

(G) Microarray data from primary SVZ neurospheres were analyzed by Spearman rank correlation computed based upon all probe sets, with red and blue representing the most and least highly correlated samples, respectively.

(H) A heatmap of 183 genes significantly differentially expressed in the datasets from (G) (using a false discovery rate [FDR] p < 0.05 and FC > 1.1 or < -1.1; listed in Table S1). Scale represents normalized gene expression values.

(I–N) Dentate gyrus sections from offspring injected with BrdU 1 day (I–M) or 1 month (N) earlier immunostained for BrdU (red in I and green in N) and/or Sox2 (green, I), doublecortin (DCX; M), or NeuN (red, N) and analyzed for the total number of Sox2-positive (J), BrdU-positive (K), Sox2-positive and BrdU-positive (L), DCX-positive (M), or BrdU-positive and NeuN-positive (N) cells. Images are from control brains. Hatched lines show the border of the SGZ, and in (I), the boxed area is shown at higher magnification. * $p < 0.05$, ** $p < 0.01$; n = 3–4 animals. In scatterplots, single points represent individual animal data.

Sections in (A), (I), and (M) were counterstained with Hoechst 33258 (blue), and arrows denote immunolabeled cells. Scale bars represent 50 μ m (A) or 20 μ m (D, I, M, and N). Error bars denote SEM. See also Figure S5.

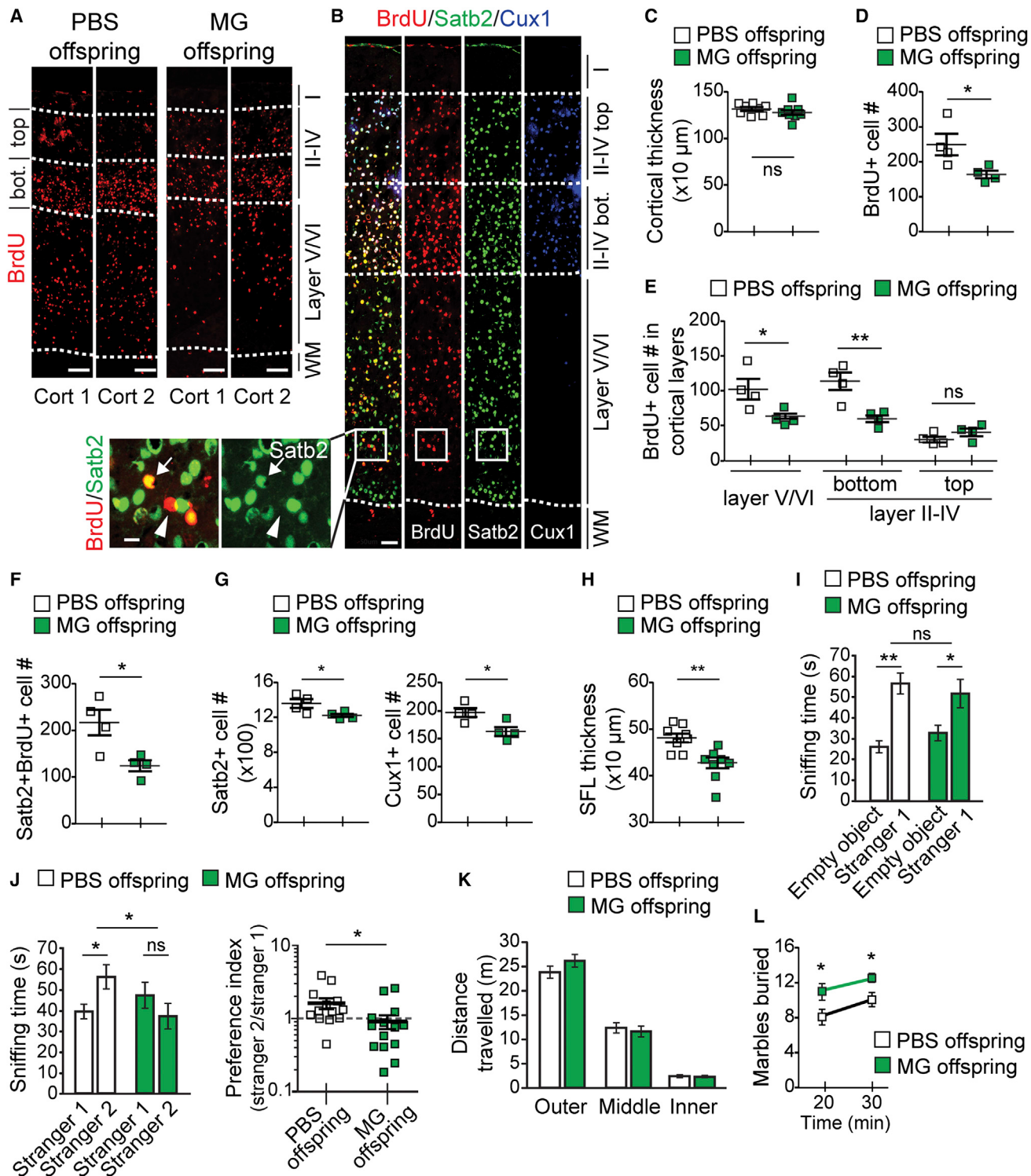


Figure 6. Embryonic Exposure to Increased Maternal Methylglyoxal Causes Long-Term Alterations in Cortical Neurons and Behavior in Adult Offspring

(A–L) Pregnant mice were injected with methylglyoxal (MG) or PBS from G12/G13 until delivery, with some mice (A–H) receiving a BrdU injection on G13/G14, and adult offspring were analyzed neuronatomiically (A–H) or behaviorally (I–L). (A–H) Cortical sections were immunostained for BrdU (red, A and B), Satb2 (green, B), and Cux1 (blue, B), and columns spanning the cortex from white matter to meninges (see Figures S6A and S6B) were analyzed for cortical thickness (C), total number of BrdU-positive cells (D), the distribution of BrdU-positive cells in different cortical layers (E), total number of BrdU-positive and Satb2-positive cells (F),

(legend continued on next page)

These findings are important in light of human epidemiological findings. In particular, human genetic variants of *Glo1* with reduced enzyme activity are associated with cognitive disorders such as ASD and schizophrenia (Junaid et al., 2004; Barua et al., 2011; Gabriele et al., 2014; Arai et al., 2010), and gestational diabetes, which induces aberrant elevation of circulating methylglyoxal (Brownlee, 2001), is linked to poor cognitive performance and ASD (Krawiak et al., 2012; Xiang et al., 2015; Li et al., 2016). The association with ASD only occurs when gestational diabetes is diagnosed on or before 26 weeks of gestation (Xiang et al., 2015), and in humans, maximal cortical neurogenesis occurs from gestational weeks 15–20 (Lui et al., 2011). Thus, the timeframe of human vulnerability corresponds to the stage of murine cortical development we have examined here.

How does increased methylglyoxal deregulate NPCs to cause these effects? The apical localization and polarity of embryonic cortical radial precursors are maintained by apical membrane proteins, including the Par polarity complex members Par3 and aPKC. Disruption of the polarized localization of these proteins causes precursors to delaminate from the apical surface and differentiate into neurons (Bultje et al., 2009; Ghosh et al., 2008). We found that when *Glo1* was decreased or methylglyoxal increased, Par3 and aPKC were reduced at the site of apical radial precursor attachment, precursors delaminated, and neurogenesis increased. How could methylglyoxal cause these changes? We propose that it does so by protein modification. Methylglyoxal is a potent glycation agent that modifies proteins and affects their functionality (Rabbani and Thornalley, 2015). If this occurred on proteins important for maintaining the neuroepithelium, then it could directly cause delamination and premature neurogenesis.

Why do methylglyoxal-induced acute alterations in embryonic NPCs cause long-lasting neural changes? The observed decrease in postnatal cortical neurons could easily be due to the premature neurogenesis and depletion of embryonic NPC pools that we document here. Moreover, since both social interactions and marble-burying involve cortical circuitry, then these perturbations in postnatal cortical neurons might account for the behavioral changes we observed. With regard to adult NPCs, it is likely that the decrease in adult SVZ NPCs is a direct consequence of the methylglyoxal-mediated decrease in embryonic cortical NPCs, which are known to contribute to the adult SVZ NPC pool (Merkele et al., 2004; Gallagher et al., 2013). This type of embryonic depletion might also explain the observed deficits in adult hippocampal NPCs, but this remains to be determined.

From a broad perspective, our results support two important concepts. First, they indicate that the maternal metabolic state normally regulates embryonic NPCs and neural development

and, conversely, that the adverse effects of a perturbed maternal environment might be mediated in part through embryonic NPCs. Second, they indicate that the size of adult SVZ and SGZ NPC pools is flexible and is determined, at least in part, by the embryonic environment, thereby providing a conceptual framework for understanding the establishment of other adult tissue stem cell pools.

EXPERIMENTAL PROCEDURES

Animals

All animal use was approved by the Animal Care Committee of the Hospital for Sick Children in accordance with the Canadian Council of Animal Care policies. All experiments used CD1 mice (Charles River Laboratory) unless otherwise specified. For methylglyoxal experiments, pregnant G12/G13 female mice were injected intraperitoneally (i.p.) twice daily with 500 µg/kg methylglyoxal (Synquest Laboratories) in PBS or PBS alone as a control. Female *Lep^{rdb/+}* mice (BKS.Cg-Dock7^{m/+} *Lep^{rdb/J}*) and wild-type C57BL/6J mice were obtained from and genotyped as indicated by Jackson Laboratory. Mice of both genders were used in all experiments. Further details are in *Supplemental Experimental Procedures*.

Cell Cultures, Transfections, and In Utero Electroporation

Cell cultures, transfections, western blots, and in utero electroporations were all performed as previously described (Yang et al., 2014; Gallagher et al., 2013). Electroporated, EGFP-positive live embryonic cortical cells were isolated by FACS on a Beckman Coulter MoFlo Astrios cell sorter (HSC Flow Cytometry Facility). For all neurosphere assays, cells were plated at one cell per microliter. Plasmids, shRNA sequences, and further details are in *Supplemental Experimental Procedures*.

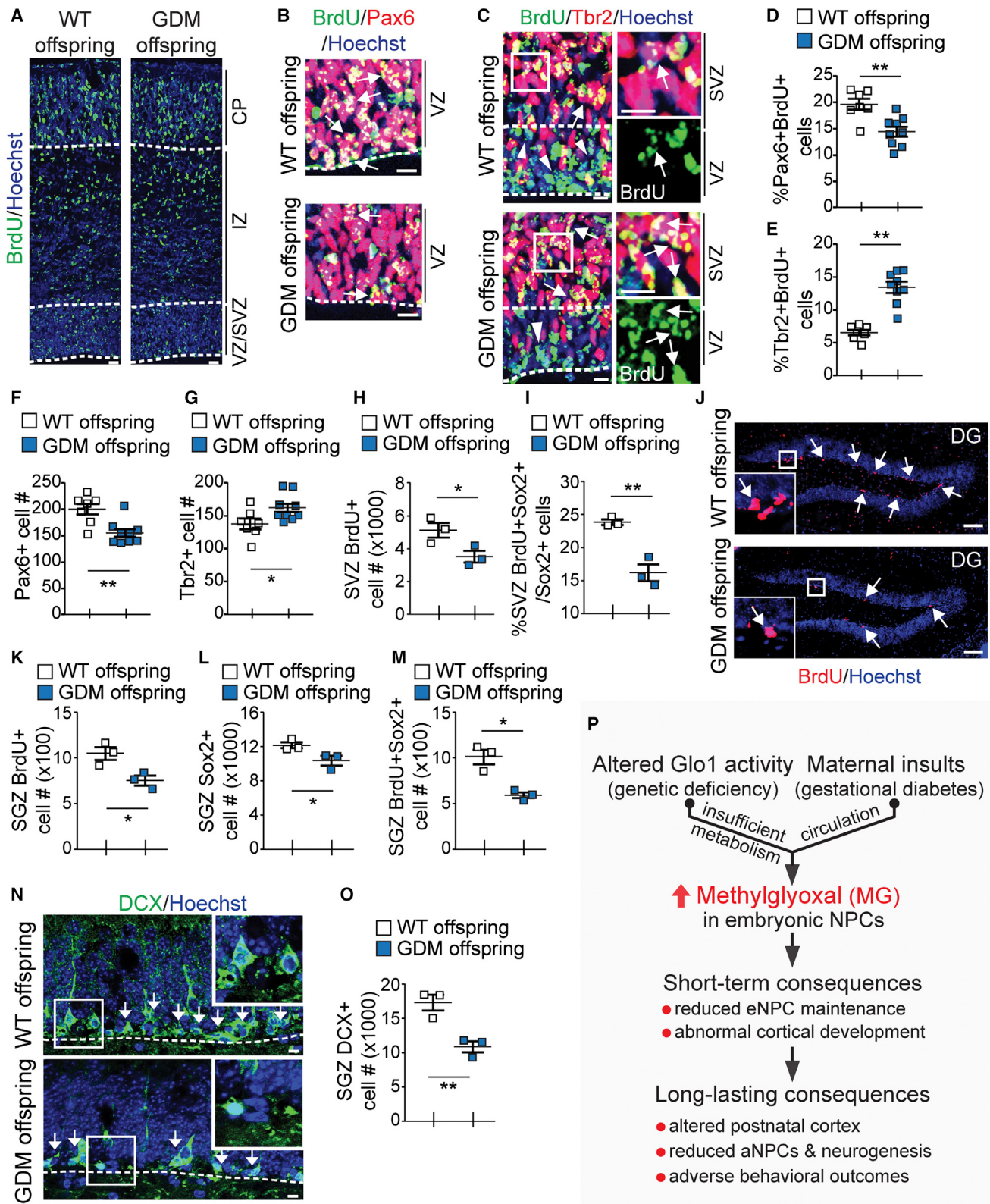
Immunostaining and FISH

Immunostaining was performed as previously described (Yang et al., 2014). Single-molecule FISH was performed with probes targeting *glo1* mRNA (NM_025374.3) using the RNAscope kit (Advanced Cell Diagnostics), according to the manufacturer's instructions. Positive signals were identified as punctate dots, and projected Z-stacks of confocal images taken with optical slice thickness of 0.1 µm are shown. Quantitative analyses were performed as previously described (Yang et al., 2014; Gallagher et al., 2013) using a Zeiss AxioPlan2 microscope and an Olympus IX81 fluorescence microscope equipped with a Hamamatsu C9100-13 back-thinned electron multiplying-charge coupled device (EM-CCD) camera and Okogawa CSU X1 spinning disk confocal scan head or with a Zeiss ApoTome2 Imaging System. Images were processed using Volocity (Perkin Elmer) or Zen software (Zeiss). Antibodies and further details are in *Supplemental Experimental Procedures*.

PCR

For RT-PCR, total cortical mRNA was isolated with the Magnetic mRNA Isolation Kit (New England Biolabs), and cDNA was synthesized with the First Strand cDNA Synthesis Kit (Thermo Scientific). For qPCR, total RNA from sorted cells was extracted using MicroElute E.Z.N.A. Total RNA Kit (Omega Biotech) and analyzed using the Quantitect Reverse Transcription Kit (QIAGEN) and a LightCycler 480 SYBR Green I Master (Roche), CFX96 Touch Real-Time

the total number of *Satb2*-positive and *Cux1*-positive cells (G), and thickness of superficial layers II–IV (SFL; H). (A) Images from two animals in each group (Cort1 and Cort2) are shown. In (A) and (B), hatched lines delineate boundaries between layer I, the top and bottom halves of layers II–IV, layer V/VI, and the white matter (WM). (B) A control brain is shown, with the boxed area shown at higher magnification, and arrows and arrowheads denote BrdU-positive cells that do and do not express *Satb2*, respectively. ns = p > 0.05, *p < 0.05, **p < 0.01; n = 4–8 animals. (I and J) Results of the three chamber social interaction assay, showing seconds spent sniffing stranger 1 versus the empty object (I), and new stranger 2 versus the old stranger 1 (J, left panel). Also shown is the preference index (time_{stranger 2}/time_{stranger 1}) for new versus old strangers (J, right). *p < 0.05, **p < 0.01; two-way ANOVA with Bonferroni's post hoc test or paired Student's t test; n = 13–14 mice. (K) Results of the open field test, showing total meters traveled in different areas in the open field. n = 11 animals each. (L) Results of the marble-burying assays, showing the number of buried marbles (of 16 total) at 20 or 30 min in the environment. *p < 0.05; Student's t test; n = 13–16 mice. In scatterplots, single points represent individual animal data. Scale bars represent 100 µm (A), 50 µm (B, low-magnification images), or 10 µm (B, high-magnification images). Error bars denote SEM. See also Figure S6.



(legend on next page)

PCR Detection System (Bio-Rad) and CFX Manager Software (Bio-Rad). All qPCR assays were performed in accordance with MIQE guidelines. Primers and further details are in [Supplemental Experimental Procedures](#).

Microarray Analyses

Total RNA was isolated using E.Z.N.A. Total RNA kit according to the manufacturer's instructions (Omega Biotek). cDNA was prepared using 250 ng total RNA and the Affymetrix Whole Transcriptome PLUS (WT PLUS) kit (Affymetrix). 5.5 µg cDNA was hybridized to the Affymetrix Gene Chip Mouse Gene 2.0 ST and results analyzed using Partek Genomics Suite 6.6. Only probe sets for annotated genes were used for differential expression analysis. ANOVA statistics were calculated and the genes with Benjamini-Hochberg p value < 0.05 and fold change (FC) > 1.1 or < -1.1 were considered statistically significant. Affymetrix Expression Console 1.1 was used for Spearman rank correlation. The heatmap.2 function of the gplots bioconductor package in R was used for the hierarchical clustering and heatmap analysis. Microarray data can be found at GEO: GSE79737.

Behavioral Assays

The social interaction test, marble-burying task, and open field assays were all performed as described in [Supplemental Experimental Procedures](#). The former two assays were manually scored by individuals blind to the treatment condition of the experimental animals, while the open field data were tracked using automated software (Limelight2, Actimetrics).

Statistics

All data are expressed as the mean ± SEM. With the exception of the microarray data, statistical analyses were performed with a two-tailed Student's t test or, where relevant, ANOVA with Tukey or Bonferroni's post hoc tests, using GraphPad Prism, unless otherwise indicated.

ACCESSION NUMBERS

The accession number for the microarray dataset reported in this paper is GEO: GSE79737.

SUPPLEMENTAL INFORMATION

Supplemental Information includes Supplemental Experimental Procedures, seven figures, and one table and can be found with this article online at <http://dx.doi.org/10.1016/j.celrep.2016.09.067>.

AUTHOR CONTRIBUTIONS

G.Y. conceptualized, designed, performed, and analyzed most of the experiments and co-wrote the paper. G.I.C. performed the adult NPC and neurogenesis experiments. S.K.Z., A.G., and A.V. designed, performed, and/or analyzed some of the experiments in the paper. D.G. helped establish the maternal methylglyoxal model. P.W.F. designed and analyzed behavioral experiments.

D.R.K. and F.D.M. conceptualized and designed experiments, analyzed data, and co-wrote the paper.

ACKNOWLEDGMENTS

This work was funded by CIHR grants MOP-125945 and 142267 and a grant from the Three to Be Foundation. F.D.M. is an HHMI Senior International Research Scholar, and F.D.M. and D.R.K. are Canada Research Chairs. G.Y., G.I.C., A.V., and D.G. were funded, respectively, by a Brain Canada Mental Health Fellowship and a SickKids Centre for Brain and Mental Health Fellowship, a Heart and Stroke Foundation of Canada Fellowship, a CIHR postdoctoral fellowship, and a McEwen Center McMurrich Fellowship. We thank Dennis Aquino for valuable technical assistance.

Received: June 19, 2016

Revised: August 8, 2016

Accepted: September 21, 2016

Published: October 18, 2016

REFERENCES

- Ankrah, N.A., and Appiah-Opong, R. (1999). Toxicity of low levels of methylglyoxal: depletion of blood glutathione and adverse effect on glucose tolerance in mice. *Toxicol. Lett.* **109**, 61–67.
- Arai, M., Yuzawa, H., Nohara, I., Ohnishi, T., Obata, N., Iwayama, Y., Haga, S., Toyota, T., Ujike, H., Arai, M., et al. (2010). Enhanced carbonyl stress in a sub-population of schizophrenia. *Arch. Gen. Psychiatry* **67**, 589–597.
- Barua, M., Jenkins, E.C., Chen, W., Kuizon, S., Pullarkat, R.K., and Junaid, M.A. (2011). Glyoxalase I polymorphism rs2736654 causing the Ala111Glu substitution modulates enzyme activity—implications for autism. *Autism Res.* **4**, 262–270.
- Brownlee, M. (2001). Biochemistry and molecular cell biology of diabetic complications. *Nature* **414**, 813–820.
- Bultje, R.S., Castaneda-Castellanos, D.R., Jan, L.Y., Jan, Y.N., Kriegstein, A.R., and Shi, S.H. (2009). Mammalian Par3 regulates progenitor cell asymmetric division via notch signaling in the developing neocortex. *Neuron* **63**, 189–202.
- Crawley, J.N. (2007). Mouse behavioral assays relevant to the symptoms of autism. *Brain Pathol.* **17**, 448–459.
- Das, R.M., and Storey, K.G. (2014). Apical abscission alters cell polarity and dismantles the primary cilium during neurogenesis. *Science* **343**, 200–204.
- Deacon, R.M. (2006). Digging and marble burying in mice: simple methods for in vivo identification of biological impacts. *Nat. Protoc.* **1**, 122–124.
- Gabriele, S., Lombardi, F., Sacco, R., Napolioni, V., Altieri, L., Tirindelli, M.C., Gregorj, C., Bravaccio, C., Rousseau, F., and Persico, A.M. (2014). The GLO1 C332 (Ala111) allele confers autism vulnerability: family-based genetic association and functional correlates. *J. Psychiatr. Res.* **59**, 108–116.

Figure 7. Maternal Diabetes Disturbs Embryonic and Adult NPC Pools in Wild-Type Offspring

(A–G) Pregnant wild-type (WT) or *Lep^{rdb/+}* (GDM) females were injected with BrdU at G13/G14, and 3 days later, cortices of embryonic wild-type progeny were immunostained for BrdU (green, A–C) and Pax6 (red, B) or Tbr2 (red, C) and analyzed for BrdU-positive cells expressing Pax6 (D) or Tbr2 (E) or for total number of Pax6-positive (F) or Tbr2-positive (G) cells in a column of defined width (see [Figure S1B](#)). In (C), boxed areas are shown at higher magnification on the right. In (B) and (C), arrows and arrowheads denote BrdU-positive cells that do or do not express cell-type-specific markers, respectively. **p < 0.01; n ≥ 7 embryos from three mothers each.

(H–O) Adult wild-type offspring of wild-type (WT) or *Lep^{rdb/+}* (GDM) mothers were injected with BrdU, and sections through the SVZ (H and I) or dentate gyrus (J–O) were immunostained 1 day later for BrdU (red, J), Sox2, and/or doublecortin (DCX; green, N). Sections were analyzed for total number of BrdU-positive SVZ cells (H), the proportion of Sox2-positive SVZ cells also positive for BrdU (I), total number of BrdU-positive SGZ cells (K), total number of Sox2-positive SGZ cells (L), total number of BrdU-positive and Sox2-positive SGZ cells (M), or total number of DCX-positive SGZ cells (O). In (J) and (N), the boxed regions are shown at higher magnification in the corners, and arrows indicate immunopositive cells. *p < 0.05, **p < 0.01; n = 3 wild-type offspring each of two mothers of each genotype. (P) Schematic of the proposed model. eNPC and aNPC refer to embryonic and adult neural precursor cells, respectively.

In scatterplots, single points represent mean cell numbers from two or three sections of an individual embryo (D–G) or individual animal data (H–O). In all images, sections were counterstained with Hoechst 33258 (blue). Scale bars represent 100 µm (A and J) or 10 µm (B, C, and N). Error bars denote SEM. See also [Figure S7](#).

- Gallagher, D., Norman, A.A., Woodard, C.L., Yang, G., Gauthier-Fisher, A., Fujitani, M., Vessey, J.P., Cancino, G.I., Sachewsky, N., Woltjen, K., et al. (2013). Transient maternal IL-6 mediates long-lasting changes in neural stem cell pools by deregulating an endogenous self-renewal pathway. *Cell Stem Cell* 13, 564–576.
- Ghosh, S., Marquardt, T., Thaler, J.P., Carter, N., Andrews, S.E., Pfaff, S.L., and Hunter, T. (2008). Instructive role of aPKC ζ subcellular localization in the assembly of adherens junctions in neural progenitors. *Proc. Natl. Acad. Sci. USA* 105, 335–340.
- Junaid, M.A., Kowal, D., Barua, M., Pullarkat, P.S., Sklower Brooks, S., and Pullarkat, R.K. (2004). Proteomic studies identified a single nucleotide polymorphism in glyoxalase I as autism susceptibility factor. *Am. J. Med. Genet. A* 131, 11–17.
- Krakowiak, P., Walker, C.K., Bremer, A.A., Baker, A.S., Ozonoff, S., Hansen, R.L., and Hertz-Pannier, L. (2012). Maternal metabolic conditions and risk for autism and other neurodevelopmental disorders. *Pediatrics* 129, e1121–e1128.
- Li, M., Fallin, M.D., Riley, A., Landa, R., Walker, S.O., Silverstein, M., Caruso, D., Pearson, C., Kiang, S., Dahm, J.L., et al. (2016). The association of maternal obesity and diabetes with autism and other developmental disabilities. *Pediatrics* 137, e20152206.
- Lui, J.H., Hansen, D.V., and Kriegstein, A.R. (2011). Development and evolution of the human neocortex. *Cell* 146, 18–36.
- Mericq, V., Piccardo, C., Cai, W., Chen, X., Zhu, L., Striker, G.E., Vlassara, H., and Uribarri, J. (2010). Maternally transmitted and food-derived glycotoxins: a factor preconditioning the young to diabetes? *Diabetes Care* 33, 2232–2237.
- Merkle, F.T., Tramontin, A.D., García-Verdugo, J.M., and Alvarez-Buylla, A. (2004). Radial glia give rise to adult neural stem cells in the subventricular zone. *Proc. Natl. Acad. Sci. USA* 101, 17528–17532.
- Mihaylova, M.M., Sabatini, D.M., and Yilmaz, Ö.H. (2014). Dietary and metabolic control of stem cell function in physiology and cancer. *Cell Stem Cell* 14, 292–305.
- Rabbani, N., and Thornalley, P.J. (2015). Dicarbonyl stress in cell and tissue dysfunction contributing to ageing and disease. *Biochem. Biophys. Res. Commun.* 458, 221–226.
- Sousa Silva, M., Gomes, R.A., Ferreira, A.E., Ponces Freire, A., and Cordeiro, C. (2013). The glyoxalase pathway: the first hundred years... and beyond. *Biochem. J.* 453, 1–15.
- Tsui, D., Vessey, J.P., Tomita, H., Kaplan, D.R., and Miller, F.D. (2013). FoxP2 regulates neurogenesis during embryonic cortical development. *J. Neurosci.* 33, 244–258.
- Villeda, S.A., Luo, J., Mosher, K.I., Zou, B., Britschgi, M., Bieri, G., Stan, T.M., Fainberg, N., Ding, Z., Eggel, A., et al. (2011). The ageing systemic milieu negatively regulates neurogenesis and cognitive function. *Nature* 477, 90–94.
- Xiang, A.H., Wang, X., Martinez, M.P., Walther, J.C., Curry, E.S., Page, K., Buchanan, T.A., Coleman, K.J., and Getahun, D. (2015). Association of maternal diabetes with autism in offspring. *JAMA* 313, 1425–1434.
- Yamashita, H., Shao, J., Ishizuka, T., Klepcyk, P.J., Muhlenkamp, P., Qiao, L., Hoggard, N., and Friedman, J.E. (2001). Leptin administration prevents spontaneous gestational diabetes in heterozygous *Lepr(db/+)* mice: effects on placental leptin and fetal growth. *Endocrinology* 142, 2888–2897.
- Yang, G., Smibert, C.A., Kaplan, D.R., and Miller, F.D. (2014). An eIF4E1/4E-T complex determines the genesis of neurons from precursors by translationally repressing a proneurogenic transcription program. *Neuron* 84, 723–739.